PHYSICAL REVIEW A **76**, 042706 (2007)

Theoretical study on electron collisions with SiF and SiF_2 radicals in the low- and intermediate-energy range

G. L. C. de Souza,[1] E. A. y Castro,[2] L. E. Machado,[2] L. M. Brescansin,[3] I. Iga,[1] and M.-T. Lee[1]
[1]*Departamento de Química, UFSCar, 13565-905 São Carlos, SP, Brazil*
[2]*Departamento de Física, UFSCar, 13565-905 São Carlos, SP, Brazil*
[3]*Instituto de Física "Gleb Wataghin," UNICAMP, 13083-970 Campinas, SP, Brazil*
(Received 29 May 2007; published 8 October 2007)

A theoretical study on electron collisions with SiF and SiF_2 radicals in the low- and intermediate-energy range is reported. More specifically, calculated elastic differential, integral, and momentum transfer cross sections as well as total and total absorption cross sections are presented in the 1–1000-eV energy range. A complex optical potential is used to represent the electron-radical interaction dynamics, whereas the iterative Schwinger variational method combined with the distorted-wave approximation is used to solve the scattering equations. Comparison of the present results with the available theoretical and experimental results in the literature is made.

DOI: 10.1103/PhysRevA.76.042706 PACS number(s): 34.80.Bm

I. INTRODUCTION

Interest in electron interactions with highly reactive radicals, such as CF_x, SiF_x ($x=1,2,3$), etc., has grown recently in view of their importance in developing plasma devices. It is well known that a plasma environment is composed of many species such as electrons, molecules (in their ground and excited states), neutral radicals, ionic fragments, etc. Knowledge of the cross sections for electron interactions with these constituents is important in determining plasma properties and therefore is useful for plasma modeling. In this sense, cross sections for e^--SiF_x ($x=1,2,3$) collisions are particularly relevant. The SiF_x radicals can be produced during plasma etching of silicon when gaseous fluorine or perfluorocarbons are used as reactant gases. Since plasma etching is one of the most fundamental processes for the manufacture of wafers in the semiconductor industry, knowledge of several cross sections for e^--SiF_x collisions is certainly relevant in order to optimize the process. The presence of such species in the reactant environment can certainly influence plasma properties. In particular, the interaction of these radicals with electrons is not very well known. Also, experimental determination of the cross sections of e^--SiF_x collisions is difficult. Only a few experimental cross sections for electron-impact ionization of these reactive radicals have been reported in the literature so far [1–3]. Theoretical investigations on electron collisions with the SiF_x radicals reported in the literature have been equally scarce. Electron-impact total ionization cross sections (TICSs) for SiF_x ($x=1,2,3$) were calculated and reported by Hwang *et al.* [4] using the semiempirical binary-encounter Bethe (BEB) approximation, by Deutsch *et al.* [5] using the Deutsch-Märk (DM) model, and by Joshipura *et al.* [6] using the additivity rule (AR). A rather complete theoretical investigation on electron interaction with the SiF radical was reported by Lee *et al.* [7] in 2002. In that study, differential (DCS), integral (ICS), and momentum-transfer (MTCS) cross sections, as well as grand-total (TCS) and total absorption (TACS) cross sections in the 1–500-eV range were reported. To our knowledge, no similar studies have ever been reported for other SiF_x radicals. Therefore, additional theoretical calculations of various cross sections for e^--SiF_x ($x=1,2,3$) collisions would certainly be interesting and could contribute to fulfill this lack.

In the study of e^--SiF scattering reported by Lee *et al.* [7], a complex optical potential composed of static-exchange, correlation-polarization, and absorption contributions was used to represent the interaction dynamics. The iterative Schwinger variational method (ISVM) [8] combined with the distorted-wave approximation (DWA) [9,10] was used to solve the scattering equations. The static-exchange part of the interaction potential was derived exactly from the target wave function. A parameter-free model suggested by Padial and Norcross [11] was used to generate the correlation-polarization potential, whereas version 3 of the quasifree scattering model (QFSM3) proposed by Staszewska *et al.* [12], and lately modified by Jain and Baluja [13], was used to account for the absorption contributions. During the last five years, our group has applied this model to account for the absorption component of the electron-molecule interaction potential. We have found that for most of the targets studied [7,14–17], the use of that optical potential can provide quite accurate DCSs, ICSs, and MTCSs for elastic electron-molecule collisions in the 10–500-eV energy range. On the other hand, such calculations have systematically underestimated the magnitudes of TCSs and TACSs, particularly at higher incident energies. The observed disagreement with experiments is probably caused by some physical origin inherently omitted in the QFSM3 formalism. In our conception, this problem could be due to the use of the free-electron gas approximation. However, in an actual scattering problem, the target electronic density is not uniform. It is expected that many-body interactions would be relevant in the region of high electronic densities and less important elsewhere. The lack of such effects could lead to distortions of the absorption potential generated by the QFSM3. In order to incorporate many-body effects, in two recent studies [18,19] we have proposed a dimensionless scaling factor, which is a function of both the incident energy and the local target density distribution, to be applied to the QFSM3 potential. It contains two parameters that were obtained through the adjustment of the calculated TACSs for N_2 at 500 eV to better

approach the experimental TICSs. This procedure can be justified because at such a high energy, the ionization process dominates the inelastic collisions and so the excitation cross sections would be negligible. This improved version of the absorption potential will be referred to as the scaled quasifree scattering model (SQFSM) potential. The SQFSM was applied to study electron collisions by a series of atomic (Ne and Ar) and molecular (N_2, C_2H_2, CO, H_2O, CH_4) targets [18,19]. The TCSs and TACSs calculated using this improved model potential agree better with the experimental data than those calculated using the QFSM3, particularly at high incident energies.

In this work, we present a theoretical study on electron scattering by the SiF and SiF_2 radicals in the low- and intermediate-energy range. Specifically, calculated DCSs, ICSs, and MTCSs as well as TCSs and TACSs are presented for electron-impact energies ranging from 1 to 1000 eV. In our study, the formalism used is the same as in [7], except that the new SQFSM is also used to represent the absorption effects. The comparison of the calculated TACSs using these model potentials with experimental and theoretical data available in the literature would provide insights of the reliability of the two model potentials.

The organization of this paper is as follows: in Sec. II, we describe briefly the theory used and also give some details of the calculation. In Sec. III, we compare our calculated results with experimental and calculated data for both e^--SiF and e^--SiF_2 scatterings available in the literature. A brief conclusion remark is also presented in that section.

II. THEORY AND CALCULATION

In this section we will briefly discuss the method used; details of the ISVM and the DWA can be found elsewhere [8–10,15,16]. Within the fixed-nuclei framework, the DCSs for electron-molecule scattering, after averaging over the molecular orientations, are given by [20]

$$\frac{d\sigma}{d\Omega} = \frac{1}{8\pi^2}\int d\alpha \sin\beta\, d\beta\, d\gamma |f(\hat{k}_i', \hat{k}_f')|^2, \tag{1}$$

where $f(\hat{k}_i', \hat{k}_f')$ is the scattering amplitude in the laboratory frame (LF), $\hat{k}_f'$ ($\hat{k}_i'$) is the direction of the scattered (incident) electron linear momentum in the LF, whereas the direction of incident electrons is taken as the LF z axis. The (α, β, γ) are the Euler angles which define the direction of the molecular principal axis. Using a closure relation, Eq. (1) can be equivalently written as

$$\frac{d\sigma}{d\Omega} = \sum_{J\tau M} \langle 000|f^*(\hat{k}_i', \hat{k}_f')|J\tau M\rangle\langle J\tau M|f(\hat{k}_i', \hat{k}_f')|000\rangle, \tag{2}$$

where $|J\tau M\rangle$ are the eigenvectors of asymmetric-top rotors and

$$\langle \hat{r}|000\rangle = (8\pi^2)^{-1/2}. \tag{3}$$

Using the adiabatic-nuclei-rotation approach, the DCS for the excitation for an asymmetric-top rotor from an initial rotational level $J\tau$ to a final level $J'\tau'$ is given by [21,22]

$$\frac{d\sigma}{d\Omega}(J\tau \to J'\tau') = \frac{1}{(2J+1)}\frac{k}{k_0}\sum_{M=-J}^{J}\sum_{M'=-J'}^{J'} |f_{J\tau M\to J'\tau' M'}|^2, \tag{4}$$

where k_0 and k are the magnitudes of the initial and final linear momenta of the scattering electrons, respectively, and $f_{J\tau M\to J'\tau' M'}$ is the rotational excitation scattering amplitude related to the target rotational eigenfunctions by

$$f_{J\tau M\to J'\tau' M'} = \langle \Psi_{J'\tau' M'}(\alpha,\beta,\gamma)|f^{LF}|\Psi_{J\tau M}(\alpha,\beta,\gamma)\rangle. \tag{5}$$

In Eq. (4), the sum over M results from the degeneracy among the eigenstates with different M. The eigenfunctions $\Psi_{J\tau M}(\alpha,\beta,\gamma)$ appearing in Eq. (5) are written as a linear combination of symmetric-top eigenfunctions [23]:

$$\Psi_{J\tau M}(\alpha,\beta,\gamma) = \sum_{K=-J}^{J} a_{KM}^{J\tau}\Phi_{JKM}(\alpha,\beta,\gamma), \tag{6}$$

where the symmetric-top eigenfunctions are given by

$$\Phi_{JKM}(\alpha,\beta,\gamma) = \left(\frac{2J+1}{8\pi^2}\right)D_{KM}^{J^*}(\alpha,\beta,\gamma) \tag{7}$$

and D_{KM}^J are the well-known Wigner rotation matrices [24]. Also, the electronic part of the LF scattering amplitude can be related to the corresponding body-frame (BF) T matrix by the usual frame transformation [24]. The latter can be conveniently partial-wave expanded as

$$T = \frac{1}{k}\sum_{p\mu lhl'h'} i^{l-l'}T_{k,lh;l'h'}^{p\mu}X_{lh}^{p\mu}(\hat{k})X_{l'h'}^{p\mu^*}(\hat{k}_0), \tag{8}$$

where $\hat{k}_0$ and $\hat{k}$ are the linear momentum directions of the incident and scattered electrons in the BF, respectively, and $X_{lh}^{p\mu}$ are the symmetry-adapted functions [25] which are expanded in terms of the usual spherical harmonics as follows:

$$X_{lh}^{p\mu}(\hat{r}) = \sum_m b_{lhm}^{p\mu}Y_{lm}(\hat{r}). \tag{9}$$

Here p is an irreducible representation (IR) of the molecular point group, μ is a component of this representation, and h distinguishes between different bases of the same IR corresponding to the same value of l. The coefficients $b_{lhm}^{p\mu}$ satisfy important orthogonality relations and are tabulated for C_{2v} and O_h point groups [25].

The rotationally unresolved DCSs for elastic e^--molecule scattering are calculated through a summation of all rotationally resolved DCSs:

$$\frac{d\sigma}{d\Omega} = \sum_{J'\tau'}\frac{d\sigma}{d\Omega}(J\tau \to J'\tau'). \tag{10}$$

Since SiF is an open-shell molecule with ground-state symmetry $X^2\Pi$, two spin-specific scattering schemes, the singlet and triplet couplings, between the scattering electron and the isolated 3π electron of the target are considered in the present study. Therefore, the statistical average of the elastic scattering DCS is written as

$$\frac{d\sigma}{d\Omega} = \frac{1}{4}\left[3\left(\frac{d\sigma}{d\Omega}\right)^1 + \left(\frac{d\sigma}{d\Omega}\right)^0\right], \tag{11}$$

where $(d\sigma/d\Omega)^1$ and $(d\sigma/d\Omega)^0$ are the multiplet-specific DCSs for the total (e^-+target) spin $S=1$ (triplet) and $S=0$ (singlet) couplings, respectively.

In our calculations, the e^--radical scattering dynamics is represented by a complex optical potential given by

$$V_{opt} = V_{SEP} + iV_{ab}, \tag{12}$$

where V_{SEP} is the real part of the optical potential composed of static (V_{st}), exchange (V_{ex}), and correlation-polarization (V_{cp}) contributions and V_{ab} is the absorption potential. V_{st} and V_{ex} are obtained exactly from a Hartree-Fock (HF) self-consistent-field (SCF) target wave function. A parameter-free model potential introduced by Padial and Norcross [11] is used to account for the correlation-polarization contributions. In this model, a short-range correlation potential between the scattering and the target electrons is defined in an inner region and a long-range polarization potential in an outer region. The first crossing of the correlation and polarization potential curves defines the inner and the outer regions. The correlation potential is calculated by a free-electron-gas model, derived from the target electronic density according to Eq. (9) of Ref. [11]. In addition, an asymptotic form of the polarization potential is used for the long-range electron-target interaction. Since there are no reported experimental dipole polarizabilities for SiF_2, calculated values at the HF-SCF level are used to generate the asymptotic form of V_{cp}. No cutoff or other adjusted parameters are needed for the calculation of the correlation-polarization contribution.

The QFSM3 absorption potential of Staszewska *et al.* [12] is given by

$$V_{ab}(\vec{r}) = -\rho(\vec{r})\left(\frac{T_L}{2}\right)^{1/2}\left(\frac{8\pi}{5k^2}k_F^3\right)H(\alpha+\beta-k_F^2)(A+B+C), \tag{13}$$

where

$$T_L = k^2 - V_{SEP}, \tag{14}$$

$$A = \frac{5k_F^3}{(\alpha - k_F^2)}, \tag{15}$$

$$B = -\frac{k_F^3[5(k^2-\beta)+2k_F^2]}{(k^2-\beta)^2}, \tag{16}$$

and

$$C = 2H(\alpha+\beta-k^2)\frac{(\alpha+\beta-k^2)^{5/2}}{(k^2-\beta)^2}. \tag{17}$$

In Eqs. (13)–(17), k^2 is the energy (in Rydbergs) of the incident electron, k_F the Fermi momentum, and $\rho(\vec{r})$ the local electronic density of the target. $H(x)$ is a Heaviside function defined by $H(x)=1$ for $x\geq 0$ and $H(x)=0$ for $x<0$. According to Staszewska *et al.* [12],

$$\alpha(\vec{r},E) = k_F^2 + 2(2\Delta - I) - V_{SEP} \tag{18}$$

and

$$\beta(\vec{r},E) = k_F^2 + 2(I-\Delta) - V_{SEP}, \tag{19}$$

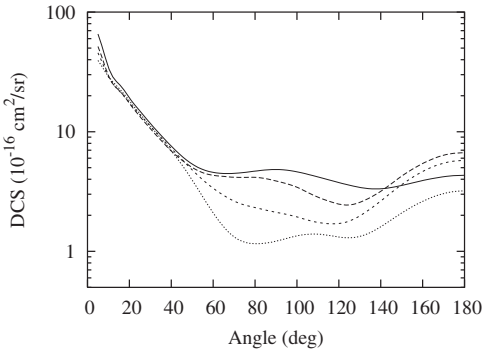

FIG. 1. DCS for elastic e^--SiF scattering calculated using only the real part of the optical potential. Solid line, results at 2 eV; dashed line, at 3 eV; short-dashed line, at 5 eV; and dotted line, at 8 eV.

where Δ is the average excitation energy and I is the ionization potential.

In the improved SQFSM version, a multiplicative dimensionless scaling factor, given as

$$F_S = 1.0 + Mkr_s - \frac{N}{kr_s}, \tag{20}$$

is applied to the QFSM3 potential. In the above equation,

$$r_s = \left[\frac{3}{4\pi\rho(\vec{r})}\right]^{1/3}. \tag{21}$$

The second and third terms on the right-hand side (rhs) of Eq. (20) account for the corrections in the low- and high-density regions, respectively. $M=0.12$ and $N=2.2$ are parameters empirically chosen. It is worth emphasizing that both M and N must depend neither on a particular target nor on a specific incident energy. The same values were used in the atomic and molecular targets in our previous works [18,19] and are also used for the targets considered herein. In the generation of both the QFSM3 and the present modified model absorption potential, the first ionization potentials (I) are used as the average excitation energies [13].

The Lippmann-Schwinger scattering equation for elastic e^--SiF_x ($x=1,2$) collisions is solved using the ISVM. In principle, this equation should be solved with the full complex optical interaction potential. Nevertheless, a tremendous computational effort would be required, particularly due to the large number of coupled equations involved, which makes such calculations practically prohibitive. On the other hand, our calculation has revealed that the magnitude of the imaginary part (absorption) of the optical potential is considerably smaller than its real counterpart. Therefore, in the present study the scattering equations are solved using the ISVM, considering only the real part of the optical potential. In ISVM calculations, the continuum wave functions are single-center expanded as

$$\chi_{\vec{k}}^{\pm}(\vec{r}) = \left[\frac{2}{\pi}\right]^{1/2}\sum_{lm}\frac{(i)^l}{k}\chi_{klm}^{\pm}(\vec{r})Y_{lm}(\hat{k}), \tag{22}$$

where the superscripts (−) and (+) denote the incoming-wave and outgoing-wave boundary conditions, respectively. Fur-

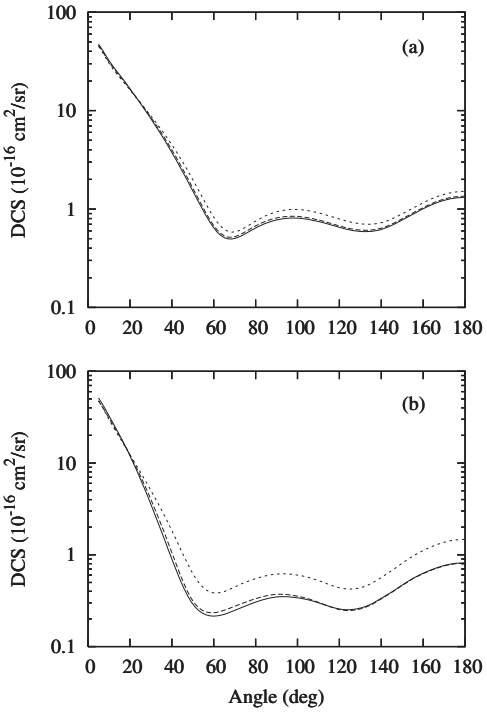

FIG. 2. DCS for elastic e^--SiF scattering at (a) 15 eV and (b) 30 eV. Solid line, present results calculated using the SQFSM; dashed line, present results calculated using the QFSM3; short-dashed line, present DCS calculated without accounting for absorption effects.

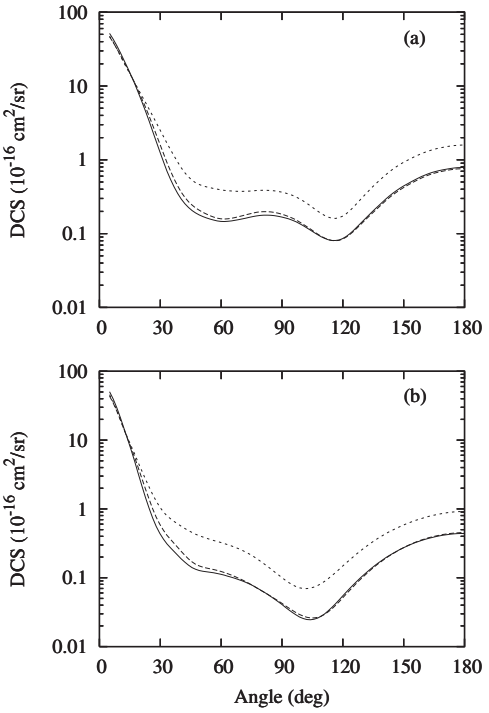

FIG. 3. Same as in Fig. 2, but for (a) 50 eV and (b) 100 eV.

thermore, the absorption part of the T matrix is calculated via the DWA as

$$T_{ab} = i\langle \chi_f^- | V_{ab} | \chi_i^+ \rangle, \tag{23}$$

where χ_f^- and χ_i^+ are distorted wave functions calculated in the ISVM. Additionally, the ICS (σ_{int}) and MTCS (σ_{mt}) are obtained directly from the integrations

$$\sigma_{int} = 2\pi \int_0^\pi \left(\frac{d\sigma}{d\Omega} \right) \sin\theta \, d\theta \tag{24}$$

and

$$\sigma_{mt} = 2\pi \int_0^\pi \left(\frac{d\sigma}{d\Omega} \right) (1 - \cos\theta) \sin\theta \, d\theta. \tag{25}$$

The TCSs (σ_{tot}) are calculated by using the optical theorem [29]. The TACSs (σ_{abs}) are calculated as the difference between TCSs and ICSs, as

$$\sigma_{abs} = \sigma_{tot} - \sigma_{int}. \tag{26}$$

The so-calculated TACSs account for the contributions from all open inelastic channels, including both excitation and ionization processes. The contributions from the electronic excitation of the target arise mainly from the low-lying dipole-allowed transitions for which cross sections become progressively small above the ionization threshold. Therefore, at sufficiently high energies, the ionization dominates the inelastic processes.

In our calculations, the partial-wave expansion of the continuum wave functions, as well as of the T-matrix elements, is limited to $l_{max}=50$ and $m_{max}=17$ for SiF and $l_{max}=23$ and $m_{max}=23$ for SiF_2. Since both targets are a polar system, these partial-wave expansions converge slowly due to the long-range dipole interaction potential. Therefore, a Born-closure formula is used to account for the contribution of higher partial-wave components to the scattering amplitudes. Accordingly, Eq. (8) is rewritten as

$$T = T^B + \frac{1}{k} \sum_{p\mu lhl'h'}^{LL'} i^{l-l'} \left(T^{p\mu\,ISVM}_{k,lh;l'h'} - T^{p\mu\,B}_{k,lh;l'h'} \right) X^{p\mu}_{lh}(\hat{k}) X^{p\mu\,*}_{l'h'}(\hat{k}_0), \tag{27}$$

where T^B is the complete point-dipole first-Born-approximation (FBA) T matrix, $T^{p\mu\,ISVM}_{k,lh;l'h'}$ are the partial-wave T-matrix elements calculated via the ISVM, and $T^{p\mu\,B}_{k,lh;l'h'}$ are the corresponding partial-wave point-dipole FBA T-matrix elements [20], given by

$$T^{p\mu\,B}_{k,lh;l'h'} = -\frac{D}{L} \left[\frac{(L+h)(L-h)}{(2L+1)(2L-1)} \right]^{1/2}, \tag{28}$$

where D is the target electric-dipole moment and $L=l'$ when $l'=l+1$ and $L=l$ when $l'=l-1$.

In this study, the wave functions of the ground-state targets are obtained using a HF-SCF calculation. The standard quantum-chemistry code GAMESS is used for these calculations. The basis functions for Si and F atoms used in the SCF calculations are presented in Table I. At the experimental equilibrium geometries, $R_{\text{Si-F}}=3.0257$ a.u. for SiF [26] and

TABLE I. Gaussian basis sets for SiF and SiF_2.

Center	*s* Exp.	*s* Coef.	*p* Exp.	*p* Coef.	*d* Exp.	*d* Coef.
Si	69989.3000	0.000750	401.6050	0.002628	1.8000	1.000000
	10380.2000	0.005941	95.3520	0.02040	0.9000	1.000000
	2330.0100	0.031099	30.3340	0.091872	0.400	1.000000
	657.4700	0.124883	10.9440	0.268204	0.13	1.000000
	214.0000	0.387915	4.0417	0.733099		
	77.6060	0.553878	4.0417	−1.107732		
	77.6060	0.177570	1.4615	1.470012		
	30.6400	0.627947	0.3302	1.000000		
	12.8160	0.247638	0.0952	1.000000		
	3.9271	1.000000	0.0140	1.000000		
	1.4522	1.000000	0.0072	1.000000		
	0.2576	1.000000	0.0035	1.000000		
	0.0944	1.000000				
	0.0480	1.000000				
	0.0170	1.000000				
	0.00425	1.000000				
F	9994.7900	0.002017	44.35550	0.020868	1.5800	1.000000
	1506.0300	0.015295	10.0820	0.130092	0.7900	1.000000
	350.2690	0.073110	2.99590	0.396219	0.3900	1.000000
	104.053	0.246420	0.93930	0.620368	0.13	1.000000
	34.8432	0.612593	0.27330	1.000000		
	4.3688	0.242489	0.0913	1.000000		
	12.2164	1.000000	0.0330	1.000000		
	1.2078	1.000000				
	0.3634	1.000000				
	0.1210	1.000000				
	0.0403	1.000000				
	0.0121	1.000000				

$R_{Si\text{-}F}=3.0049$ a.u. and $\theta=100.77°$ for SiF_2 [27], the calculated HF-SCF energy and the dipole moment are −388.3223 a.u. and 0.981 D, respectively, for SiF, which can be compared to the values of −388.41575 a.u. and 1.20 D of O'Hara and Wahl [28]. The corresponding values for SiF_2 are −487.9847 a.u. and 1.12 D, respectively. The experimental dipole moment for this radical is 1.23 D [26]. The calculated dipole polarizabilities are $\alpha_{xx}=\alpha_{yy}=38.503$ a.u. and $\alpha_{zz}=27.815$ a.u. for SiF and $\alpha_{xx}=33.534$ a.u., $\alpha_{yy}=50.351$ a.u., and $\alpha_{zz}=30.772$ a.u. for SiF_2. Unfortunately, there are no experimental or other calculated values for comparison.

III. RESULTS AND DISCUSSION

A. Electron scattering by the SiF radical

Figure 1 shows the rotationally summed DCSs for elastic e^--SiF scattering at incident energies of 2, 3, 5, and 8 eV calculated using only the real part of the optical potential. At such low energies, almost no inelastic scattering channels are open and therefore no absorption effects need to be included in the calculations. Unfortunately, the lack of experimental and/or other theoretical data has limited our discussions. It is seen that the angular behavior of the DCSs are highly energy dependent. All the DCSs are strongly forward peaked, reflecting the dipolar nature of the target. In Figs. 2–4 we present our rotationally summed DCSs calculated using both the QFSM3 and the SQFSM in the 15–500-eV energy range. Calculated results without accounting for absorption effects are also shown for comparison. The DCSs calculated using both the original QFSM3 potential and the SQFSM agree very well with each other even at incident energies as high as 500 eV. At 15 eV, the results obtained without absorption effects also agree well with the other two calculated results, indicating that the absorption effects are still very small at this incident energy, which is in fact expected. On the other hand, at higher energies, the DCSs calculated without accounting for the absorption effects lie systematically above those calculated including these effects.

In Figs. 5(a) and 5(b) we show our spin-averaged ICSs and MTCSs, respectively, calculated using both the SQFSM

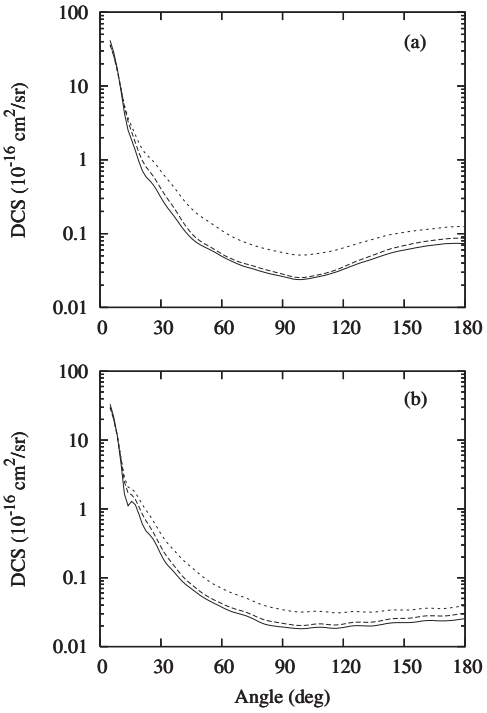

FIG. 4. Same as in Fig. 2, but for (a) 300 eV and (b) 500 eV.

and the QFSM3, in the 1–1000-eV energy range, along with those obtained without absorption effects. Our calculations have shown a shoulder at about 3 eV in both ICSs and MTCSs. This feature is in fact the same resonance reported

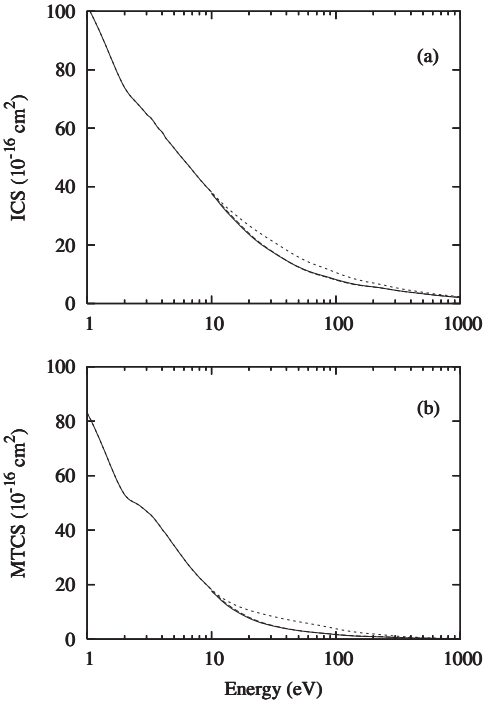

FIG. 5. (a) ICS and (b) MTCS for elastic e^--SiF scattering in the 1–1000-eV energy range. Solid line, present results calculated using the SQFSM; dashed line, present results calculated using the QFSM3; short-dashed line, present DCS calculated without accounting for absorption effects.

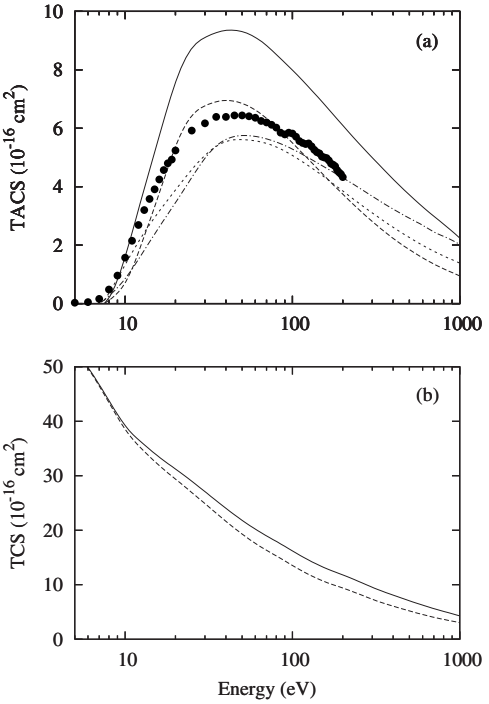

FIG. 6. (a) TACSs and (b) TCSs for electron scattering by SiF in the 5–1000-eV energy range. Solid line, present results calculated using the SQFSM; dashed line, present results calculated using the QFSM3; short-dashed line, calculated TICSs of Hwang *et al.* using the BEB approximation; dash-dotted line, calculated TICSs of Joshipura *et al.* [6] using the AR; solid circles, experimental TICS of Hayes *et al.* [3].

by Lee *et al.* [7]. Eigenphase-sum analyses have shown that the shoulder is due to a combination of a shape resonance in the $k^1\Pi$ scattering channel, centered at about 1.5 eV with width of 1.2 eV, and a broad shape resonance in the $k^3\Delta$ channel located at about 3.5 eV with width of 4 eV. At energies below 10 eV, the ICSs and MTCSs calculated with or without accounting for absorption effects are almost identical. Nevertheless, at higher energies, the results calculated without absorption effects are considerably larger than those obtained when absorption effects are included, particularly at incident energies above 30 eV. On the other hand, the cross sections calculated by using both QFSM3 and SQFSM agree quite well with each other in the entire energy range covered herein.

Figures 6(a) and 6(b) present our TACSs and TCSs, respectively, calculated using both the SQFSM and the QFSM3 in the 5–1000-eV range. The experimental TICSs of Hayes *et al.* [1] as well as the calculated TICSs of Hwang *et al.* [4] using the BEB approximation and the calculated TICSs of Joshipura *et al.* [6] using the AR are also shown in Fig. 6(a) for comparison. It is interesting to note that although the DCSs, ICSs, and MTCSs calculated using both model absorption potentials in general agree very well with each other at the energies covered herein, the calculated TACSs and TCSs are quite different. Indeed, the TACSs obtained using the SQFSM are systematically larger than those calculated using the QFSM3, particularly at higher incident energies. Moreover, our calculated TACSs show a good

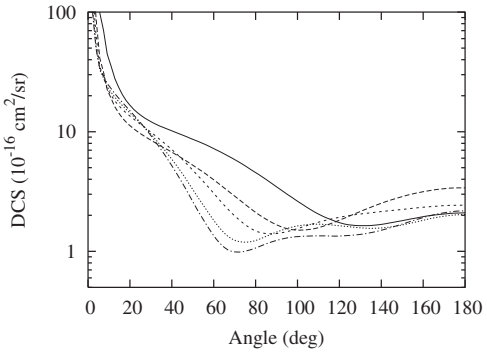

FIG. 7. DCS for elastic e^--SiF_2 scattering calculated using only the real part of the optical potential. Solid line, results at 1 eV; dashed line, at 3 eV; short-dashed line, at 5 eV; dotted line, at 8 eV; dot-dashed line, at 10 eV.

qualitative agreement with the experimental and calculated TICSs. Quantitatively, our SQFSM TACSs are about 30% larger than the experimental and calculated TICSs near the maximum, but the difference between our SQFSM TACSs and the BEB TICSs and AR TICSs decreases with increasing energies. This fact seems to be quite plausible, since all inelastic processes, including excitation and ionization, are accounted for in the absorption potential. Therefore, the calculated TACSs should establish an upper limit for the TICSs. In fact, Joshipura *et al.* [6] have verified that for a series of stable molecules such as O_2, H_2O, CH_4, SiH_4, etc., for which experimental TICSs are known accurately [30], the ionization processes are about 70%–80% of all inelastic processes at incident energy where the calculated TACSs attains its maximum. This observation is in accordance with our TACSs calculated using the SQFSM. On the other hand, the QFSM3 TACSs lie below both calculated TICSs at high incident energies, which seems to be unreasonable.

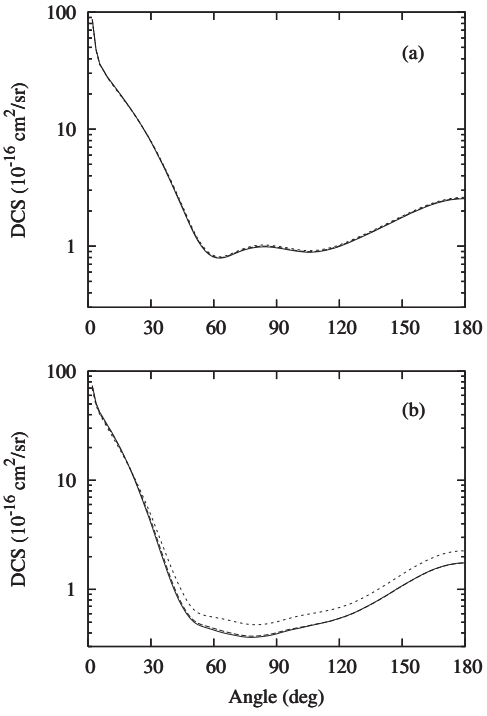

FIG. 8. DCS for elastic e^--SiF_2 scattering at (a) 15 eV and (b) 30 eV. Solid line, present results calculated using the SQFSM; dashed line, present results calculated using the QFSM3; short-dashed line, present DCS calculated without accounting for absorption effects.

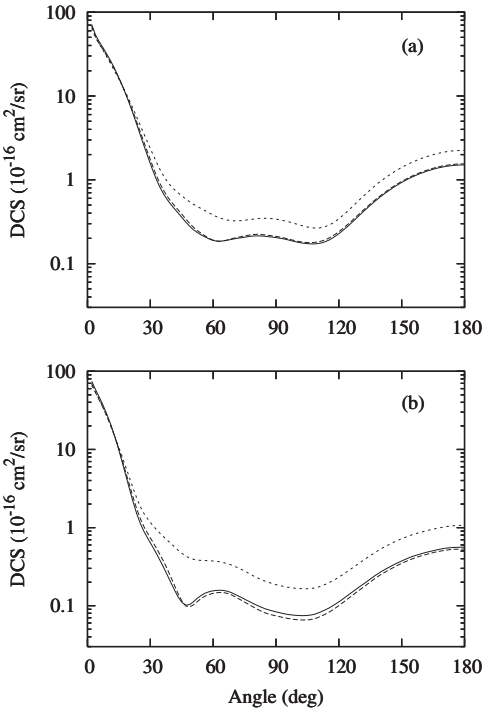

FIG. 9. Same as in Fig. 8, but for (a) 50 eV and (b) 100 eV.

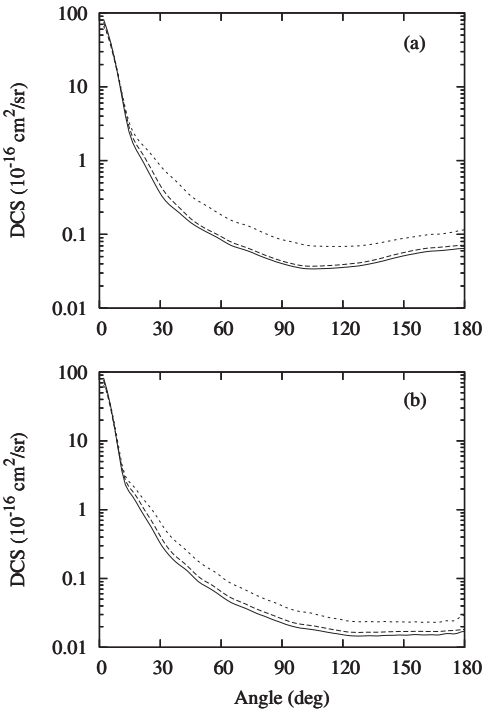

FIG. 10. Same as in Fig. 8, but for (a) 300 eV and (b) 500 eV.

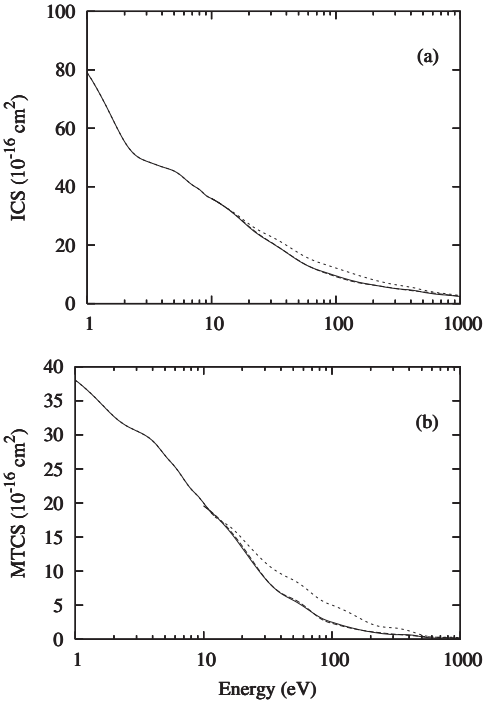

FIG. 11. (a) ICSs and (b) MTCSs for elastic e^--SiF_2 scattering in the 1–1000-eV energy range. Solid line, present results calculated using the SQFSM; dashed line, present results calculated using the QFSM3; short-dashed line, present DCS calculated without accounting for absorption effects.

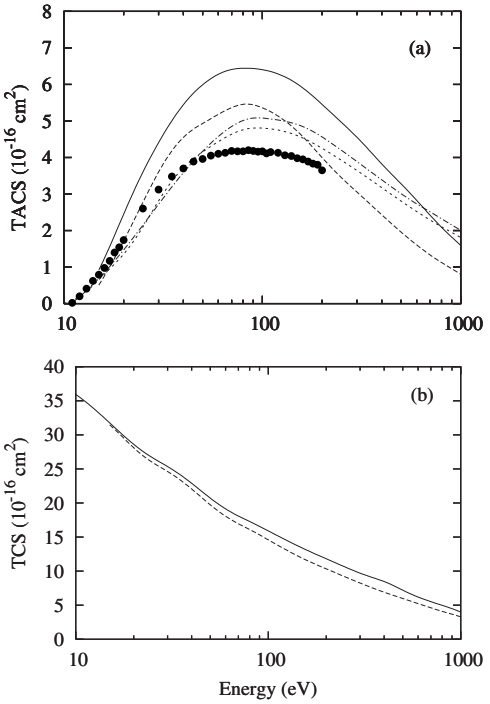

FIG. 12. (a) TACSs and (b) TCSs for electron scattering by SiF_2 in the 10–1000-eV energy range. Solid line, present results calculated using the SQFSM; dashed line, present results calculated using the QFSM3; short-dashed line, calculated TICSs of Hwang *et al.* using the BEB approximation; dash-dotted line, calculated TICSs of Joshipura *et al.* [6] using the AR; solid circles, experimental TICSs of Shul *et al.* [2].

B. Electron scattering by the SiF_2 radical

In Fig. 7 we present our rotationally summed DCS for elastic e^--SiF_2 scattering at 1, 3, 5, 8, and 10 eV. As in the case of SiF, the angular behavior of the DCSs in this low-energy range is very sensitive to the incident energy. Also, the rapid enhancement of DCSs at angles towards the forward direction is due to the dipolar nature of the target. Figures 8–10 show our rotationally summed DCS for elastic e^--SiF_2 scattering, calculated using both the QFSM3 and the SQFSM in the 15–500-eV energy range along with the DCSs calculated without accounting for absorption effects. Similar to what was observed for SiF, it is seen that the DCSs calculated using both the original QFSM3 and the SQFSM potentials agree very well with each other even at incident energies as high as 500 eV. Again at 15 eV, the results obtained without absorption effects also agree well with those calculated results including such effects, but become substantially larger at higher energies.

In Figs. 11(a) and 11(b), we show our ICSs and MTCSs for elastic e^--SiF_2 scattering, calculated using both the SQFSM and the QFSM3 in the 1–1000-eV energy range, along with those obtained without absorption effects. The conclusion is again similar to what has been observed in the case of e^--SiF collisions: the results obtained by using both absorption potentials agree quite well with each other in the entire energy range covered herein, whereas considerably larger ICSs and MTCSs are obtained without absorption effects, in particular at incident energies above 30 eV. Also for e^--SiF_2 scattering, a shoulder at around 5 eV is clearly shown in both ICSs and MTCSs. According to the eigenphase-sum analyses (not shown), we have attributed this feature to the occurrence of a shape resonance in the k^2 B_2 scattering channel located at about 5.5 eV with width of 1 eV.

Figures 12(a) and 12(b) present our TACSs and TCSs, respectively, calculated using both the SQFSM and the QFSM3 in the 10–1000-eV range. The experimental TICSs of Shul *et al.* [2] as well as the calculated TICSs of Hwang *et al.* [4] using the BEB approximation and of Joshipura *et al.* [6] using the AR are also shown in Fig. 12(a) for comparison. As expected, the TACSs obtained using SQFSM are systematically larger than those calculated using the QFSM3, particularly at higher incident energies. Also, our calculated TACSs using both absorption model potentials agree qualitatively well with the experimental TICSs. As expected, the SQFMS TACSs are, in general, larger than the experimental and calculated TICSs. The factor of 70% between the experimental TICSs and our SQFMS TACSs near the maximum is again approximately verified.

In summary, the present work performed studies of electron collisions with two important radicals, SiF and SiF_2, in a wide energy range. Our study revealed important influence of the inelastic processes on the elastic electron collisions with these targets. These effects reduce significantly the DCSs, ICSs, and MTCSs, particularly for incident energies above 30 eV. Also, we verified that the TACSs calculated using the original QFSM3 are in general smaller than the

experimental and calculated TICSs at energies above 300 eV, which is unphysical. This failure, mainly caused by the neglect of many-body interactions, can be adequately corrected by using the SQFSM.

ACKNOWLEDGMENTS

This work was partially supported by the Brazilian agencies FAPESP and CNPq.

[1] T. R. Hayes, R. C. Wetzel, F. A. Baiocchi, and R. S. Freund, J. Chem. Phys. **88**, 823 (1988).
[2] R. J. Shul, T. R. Hayes, R. C. Wetzel, F. A. Baiocchi, and R. S. Freund, J. Chem. Phys. **89**, 4042 (1988).
[3] T. R. Hayes, R. J. Shul, F. A. Baiocchi, R. C. Wetzel, and R. S. Freund, J. Chem. Phys. **89**, 4035 (1988).
[4] W. Hwang, Y.-K. Kim, and M. E. Rudd, J. Chem. Phys. **104**, 2956 (1996).
[5] H. Deutsch, C. Cornelissen, L. Cespiva, V. Bonacic-Koutecky, D. Margreiter, and T. D. Märk, Int. J. Mass Spectrom. Ion Process. **129**, 43 (1993).
[6] K. N. Joshipura, M. Vinodkumar, B. K. Antony, and N. J. Mason, Eur. Phys. J. D **23**, 81 (2003).
[7] M.-T. Lee, M. F. Lima, A. M. C. Sobrinho, and I. Iga, Phys. Rev. A **66**, 062703 (2002).
[8] R. R. Lucchese, G. Raseev, and V. McKoy, Phys. Rev. A **25**, 2572 (1982).
[9] A. W. Fliflet and V. McKoy, Phys. Rev. A **21**, 1863 (1980).
[10] Mu-Tao Lee and V. McKoy, Phys. Rev. A **28**, 697 (1983).
[11] N. T. Padial and D. W. Norcross, Phys. Rev. A **29**, 1742 (1984).
[12] G. Staszewska, D. W. Schwenke, and D. G. Truhlar, Phys. Rev. A **29**, 3078 (1984).
[13] A. Jain and K. L. Baluja, Phys. Rev. A **45**, 202 (1992).
[14] M.-T. Lee, M. F. Lima, A. M. C. Sobrinho, and I. Iga, J. Phys. B **35**, 2437 (2002).
[15] A. M. C. Sobrinho, N. B. H. Lozano, and M.-T. Lee, Phys. Rev. A **70**, 032717 (2004).
[16] M.-T. Lee, I. Iga, M. G. P. Homem, L. E. Machado, and L. M. Brescansin, Phys. Rev. A **65**, 062702 (2002).
[17] L. M. Brescansin, P. Rawat, I. Iga, M. G. P. Homem, M.-T. Lee, and L. E. Machado, J. Phys. B **37**, 471 (2004).
[18] M.-T. Lee, I. Iga, L. E. Machado, L. M. Brescansin, E. A. y Castro, I. P. Sanches, and G. L. C. de Souza, J. Electron Spectrosc. Relat. Phenom. **155**, 14 (2007).
[19] E. A. y Castro, G. L. C. de Souza, I. Iga, L. E. Machado, L. M. Brescansin, and M.-T. Lee, J. Electron Spectrosc. Relat. Phenom. **195**, 30 (2007).
[20] T. N. Rescigno and B. H. Lengsfield, Z. Phys. D: At., Mol. Clusters **24**, 117 (1992).
[21] D. M. Chase, Phys. Rev. **104**, 838 (1956).
[22] A. Jain and D. G. Thompson, J. Phys. B **16**, 3077 (1983).
[23] A. Jain and D. G. Thompson, Comput. Phys. Commun. **30**, 301 (1983).
[24] M. E. Rose, *Elementary Theory of Angular Momentum* (Wiley, New York, 1957).
[25] P. G. Burke, N. Chandra, and F. A. Gianturco, J. Phys. B **5**, 2212 (1972).
[26] *Handbook of Chemistry and Physics*, 73rd ed., edited by D. V. Lide (CRC Press, Boca Raton, FL, 1993).
[27] J. Karolczak, R. H. Judge, and D. J. Clouthier, J. Am. Chem. Soc. **117**, 9523 (1995).
[28] P. A. G. O'Hara and A. C. Wahl, J. Chem. Phys. **55**, 666 (1971).
[29] C. J. Joachain, *Quantum Collision Theory* (North-Holland, Amsterdam, 1983).
[30] G. P. Karwasz, R. S. Brusa, and A. Zecca, Riv. Nuovo Cimento **24**, 1 (2001).